

RAR-U-Net: A RESIDUAL ENCODER TO ATTENTION DECODER BY RESIDUAL CONNECTIONS FRAMEWORK FOR SPINE SEGMENTATION UNDER NOISY LABELS

Ziyang Wang¹, Zhengdong Zhang², Irina Voiculescu¹

¹Department of Computer Science, University of Oxford, UK

² State Key Laboratory of Virtual Reality Technology and Systems, Beihang University, China

ABSTRACT

Segmentation algorithms of medical image volumes are widely studied for many clinical and research purposes. We propose a novel and efficient framework for medical image segmentation. The framework functions under a deep learning paradigm, incorporating four novel contributions. Firstly, a residual interconnection is explored in different scale encoders. Secondly, four copy and crop connections are replaced to residual-block-based concatenation to alleviate the disparity between encoders and decoders, respectively. Thirdly, convolutional attention modules for feature refinement are studied on all scale decoders. Finally, an adaptive denoising learning strategy(ADL) based on the training process from underfitting to overfitting is studied. Experimental results are illustrated on a publicly available benchmark database of spine CTs. Our segmentation framework achieves competitive performance with other state-of-the-art methods over a variety of different evaluation measures.

Index Terms— Semantic Segmentation, Computed Tomography, U-Net, Spine

1. INTRODUCTION

Encoder-decoder has been one of the most prominent deep neural network architectures used in medical image segmentation. U-Net [1] is a completely symmetric variety of encoder-decoder. The encoder extracts pixel location features with down sampling; the decoder recovers the spatial dimension and pixel location features with deconvolution. Between the encoder and decoder layer there is a copy and crop connection. The optimized high resolution Dense-U-Net Network for spine segmentation proposed by Kolařík et al. [2] explores the performance of 2D and 3D U-Nets in residual networks and densely connected networks. Due to the 3D convolutional layers and interconnections, this architecture is costly in training parameter time.

A separate hurdle when segmenting medical data is the potential lack of precision in the annotated contours, usually due to the scarcity of radiographer time. As a result, results of the annotation process can depart from the the gold standard: labelled features can present slight erosion or dilation of what

would be the ideal contours, as well as various kinds of elastic transformations. We hereafter call such variations ‘noisy labels’.

In this work, we propose to overcome the shortcomings described above through RAR-U-Net, a **R**esidual encoder to **A**ttention decoder by **R**esidual connections framework, for medical image segmentation under noisy labels. Its novelty consists of: (1) shortcut interconnections on four down-sampling blocks as residual encoders, (2) a residual-block-based concatenation which mitigates the disparity with easier learning tasks, (3) a convolutional attention module on four up-sampling blocks, and (4) an adaptive denoising learning strategy which mitigates variation in hand annotations.

2. METHODS

The architecture of RAR-U-Net is illustrated in Fig. 1. Its backbone is an encoder-decoder. A symmetrical architecture which consists of convolutional, deconvolutional, upsampling, and downsampling allows to contract and recover pixel-level information. We detail below the four specific aspects of this architecture.

2.1. Residual Interconnections Networks

Inspired by ResNet [3], a concatenation function is designed in each down-sampling block. In order to strengthen the ability to express features, after obtaining the downsampled features of the previous layer, these features will go through a new feature extraction process. The extraction process consists of the repeated application of two 3×3 unpadded convolutions, each followed by a rectified linear unit (ReLU). The number of feature channels is doubled compared with previous layer after the first 3×3 convolution operator. At the end we concatenate the downsampled feature with the feature acquired from the second 3×3 convolution operator. This operation aims to establish connections between different layers, making full use of feature information and alleviating the problem of gradient disappearance.

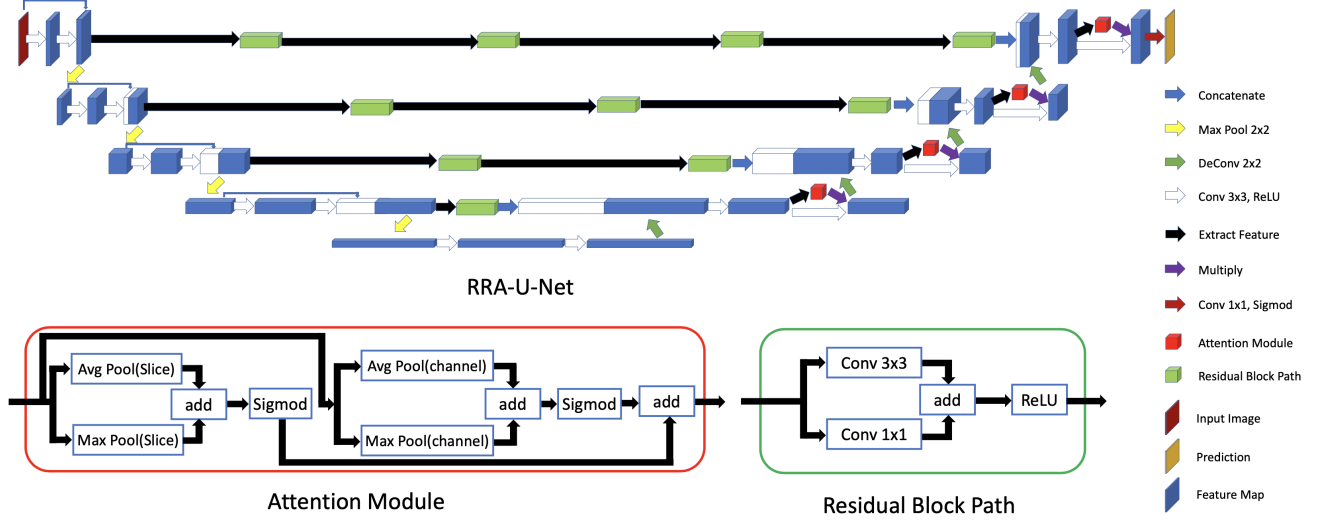


Fig. 1: The Architecture of the Proposed RAR-U-Net Network, Attention Module and Residual Block Path

2.2. Residual-Block-Based Connection Paths

Considering the disparity between encoders and decoders which may degrade the segmentation performance [4]. The four copy and crop connections are replaced by residual-block-based concatenation to alleviate the disparity between encoders and decoders in each layer, respectively. We adopt residual learning to connect encoder to decoder in each layer.

We define the Residual Block Path as a building block of our model, also sketched in Fig. 1. Formally, if x and y are the input and output vectors of the layers considered, then

$$y = F(x, \{W_i\}) + x \quad (1)$$

The function $F(x, \{W_i\})$ represents the residual mapping to be learned. For the example in Fig. 1 that has one 3×3 layer, $F = \sigma W_1 x$ in which σ denotes ReLU; to simplify notation, the biases are omitted. The operation $F + x$ is performed by a shortcut connection and element-wise addition. We also use a 1×1 convolution operator to match the number of channels.

After the addition operation we adopt the second non-linearity ReLU. Finally, the feature map processed through the residual block is concatenated with the upsampled feature of the decoder. The number of Residual Blocks at each level of the encoder-decoder is 4, 3, 2 and 1, respectively.

2.3. Convolutional Attention Module

To enhance the performance of the decoder classification for each pixel in the presence of noisy labels, we explore the use of an attention mechanism. Unlike attention gate filter features from skip connections [5], an attention module can normally be integrated with convolutional layers to enhance key information of the feature map with pooling layers and sigmoid activation functions [6].

Our proposed attention module for the convolutional layer of decoder is also sketched in Fig. 1. There are two parts to the attention, related to the channel and the slice of each feature map. Both attention parts are developed for the pooling layer and sigmoid activation. Average and max pooling layers avoid noisy label gradients to update trunk parameters. The sigmoid function allows for the output to depend on the weight attention value for each pixel location.

Fig. 1 shows how a feature map $F \in R^{W \times H \times D}$ from a previous CNN is sent to the attention module pipeline. The feature maps from the average pooling layers and max pooling layers on the dimensions of the slice are denoted F_{Slice}^{Avg} and $F_{Slice}^{Max} \in R^{W \times H \times 1}$. Similarly, $F_{Channel}^{Avg}, F_{Channel}^{Max} \in R^{1 \times 1 \times D}$ are the feature maps from average pooling layers and max pooling layers on the dimension of the channel.

The final output of the weight attention value W is calculated from the above feature maps through the sigmoid activation σ . It can then be multiplied with specific features.

$$W = \sigma(F_{Slice}^{Avg} + F_{Slice}^{Max}) + \sigma(F_{Channel}^{Avg} + F_{Channel}^{Max}) \quad (2)$$

2.4. Adaptive Denoising Learning

In order to deal with the realistic challenge of noisy labels emerging from practical settings, we propose a strategy of adaptive denoising to be applied during training. To simulate this, a certain proportion β of masks in the training data have been replaced with noisy labels. These labels present with erosions, dilations or elastic transforms. The noise is present to a smaller or greater extent denoted $\alpha \in (0..1)$. Three such noisy label examples are illustrated in Fig. 2c, 2d, 2e. The

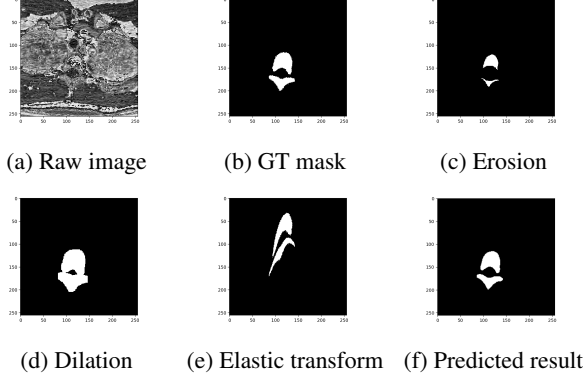


Fig. 2: Example of spine CT slice and its alterations

noise level α can be thought of as the Dice overlap measure between the original training data and the noisy label data.

We propose a simple and efficient adaptive denoising learning method. Inspired by O2U-Net [7], the losses of each label are recorded while training. The higher the loss of a label, the higher its probability of being noisy label. During training, our strategy allows to detect and remove a number of high loss value labels. A large number of noisy labels get detected at the beginning of the iteration, and then several more at the end. This is because the training process evolves from underfitting to overfitting. The number $N(t)$ of labels detected and removed in each epoch is

$$N(t) = \begin{cases} 0.5(1 - \alpha)\beta y, & 0 < t < 0.1(1 - \alpha)\beta x \\ \frac{y}{x}t, & 0.1(1 - \alpha)\beta x \leq t \leq 0.5(1 - \alpha)\beta x \\ 0.1(1 - \alpha)\beta y, & 0.5(1 - \alpha)\beta x \leq t \leq x \end{cases} \quad (3)$$

where t is the training epoch, α is the level noise, β is the proportion of items in the training dataset to which noise has been applied, x is the total number of training epochs, and y is the total number of masks.

3. EXPERIMENTS AND RESULTS

3.1. Dataset and Experimental Setup

We used a spine dataset which consists of CT scans from 10 patients, of up to 600 slices per scan, at a resolution of 512×512 , and 1mm inter-slice spacing. All images are normalized and resized to 256×256 . Ground truth (GT) masks are associated with every image, some of which were used as input for the noise introduction.

The RAR-U-Net code was developed in Python using Tensorflow. It has been run on an Nvidia GeForce RTX2080 Ti GPU with 16GB memory, and Intel(R) Xeon(R) CPU E5-2650 v4. The runtimes varied between 1000 and 1200 mins. With a training batch size of 8, the learning rate is 10^{-5} . Given the imbalance between the spine and background pixels, the loss function was based on the Dice coefficient. The

Table 1: Direct comparison against existing algorithms

Model	Dice	Acc	Pre	Rec	Spe	Par 10^6
UNet	0.8360	0.9863	0.8832	0.7936	0.9952	7.76
Residual-UNet	0.8810	0.9898	0.9097	0.8540	0.9961	9.90
Densely-UNet	0.8316	0.9860	0.8832	0.7857	0.9952	15.47
M-UNet	0.9478	0.9954	0.9512	0.9444	0.9978	7.77
M-Densely-UNet	0.9517	0.9958	0.9524	0.9508	0.9978	15.48
VGG16 UNet	0.9138	0.9925	0.9235	0.9043	0.9966	23.75
ResNet34 UNet	0.6626	0.9689	0.6333	0.6947	0.9815	24.45
SE-ResNet34 UNet	0.7306	0.9762	0.7265	0.7347	0.9873	24.61
ResNeXt101 UNet	0.7597	0.9765	0.6909	0.8438	0.9826	32.06
DenseNet121 UNet	0.7982	0.9811	0.7526	0.8498	0.9872	12.13
InceptionV3 UNet	0.8109	0.9837	0.8250	0.7972	0.9922	29.93
EfficientNet UNet	0.8358	0.9857	0.8431	0.8286	0.9929	10.11
MultiRes UNet	0.8542	0.9864	0.8094	0.9043	0.9902	7.26
LinkNet	0.8958	0.9908	0.8919	0.8999	0.9950	20.32
FPN	0.8804	0.9893	0.8675	0.8936	0.9937	17.59
3D UNet	0.8078	0.9874	0.7788	0.8390	0.9922	22.58
3D Residual-UNet	0.7757	0.9850	0.7360	0.8198	0.9904	28.15
3D Densely-UNet	0.7921	0.9860	0.7450	0.8456	0.9906	44.78
3D Attention UNet	0.8623	0.9870	0.8129	0.9182	0.9902	22.60
RAR-U-Net	0.9580	0.9963	0.9605	0.9554	0.9982	11.79

Table 2: Difference measures of the segmentation results

	HD (pixels)	ASSD	RVD
RAR-U-Net	10.0110	0.8221	0.0518

training epochs setting is illustrated in Section 2.4. Some of the benchmarks are developed by an open source library [8].

3.2. Results and Discussion

Fig. 2a, 2b, and 2f illustrate an example raw image, GT mask and average predicted result. We first compare the performance of our algorithm against a collection of others using conventional, widely used overlap measures such as the Dice coefficient, Sensitivity or Recall, Specificity, Precision, Accuracy are illustrated in Table 1, together with the number of training parameters. We also study the performance of our algorithm through difference measures such as the Hausdorff Distance, the Average Symmetric Surface Distance (ASSD) and the Relative Volume Difference (RVD), with the results listed in Table 2.

Additionally, we study the extent to which the boundaries of the predicted masks match those of the GT [9]. We report all of the Directed Boundary Dice relative to GT (DBD_G), Directed Boundary Dice relative to MS (DBD_M) and Symmetric Boundary Dice (SBD). In a von Neumann neighbourhood N_x of each pixel x on the boundary ∂G of the ground

Table 3: Boundary-based match in the segmentation results

	DBD _G	DBD _M	SBD
RAR-U-Net	0.8425	0.8564	0.8465

Table 4: Ablation Studies on Contributions of Architecture

Residual Encoders	Residual Connections	Attention Decoders	Dice	Acc	Trainable Parameters
			0.8360	0.9863	7,762,465
✓			0.9489	0.9954	9,899,625
	✓		0.9539	0.9960	8,912,673
		✓	0.9433	0.9950	7,785,157
✓		✓	0.9513	0.9957	9,922,317
✓	✓		0.9543	0.9960	11,049,833
✓	✓	✓	0.9580	0.9963	11,794,125

truth, $DBD_G = DBD(G, M) = \frac{\sum_{x \in \partial G} \text{Dice}(N_x)}{|\partial G|}$, and $SBD = \frac{\sum_{x \in \partial G} DSC(N_x) + \sum_{y \in \partial M} DSC(N_y)}{|\partial G| + |\partial M|}$. These measures penalise mislabelled areas in the machine segmentation. Even a 75% close match between the boundaries is considered a good result. Table 3 reports these.

3.3. Ablation study

In order to analyze the effects of each of the four proposed contributions and their combinations, extensive ablation experiments have been conducted. Table 4 documents how the removal of one or more components compromises the overall performance. The same table also gives a measure of the complexity of the overall RAR-U-Net model and its submodels by listing the total number of trainable parameters. Table 5 focuses specifically on the effect of the ADL strategy on different levels of noisy labels in the data.

4. CONCLUSIONS

All four proposed contributions significantly improve both the segmentation performance and the training parameter cost. Although the tests were specific to a single dataset, the methods are, of course, generic.

5. COMPLIANCE WITH ETHICAL STANDARDS

This is a study for which no ethical approval was required. The spine dataset is open public and provided by the University of California and National Institutes of Health [10]. There is no financial and personal relationships of the author

Table 5: Ablation Studies on ADL

Proportion	Level	Algorithm	ADL	Dice	Acc
75%	0.68	U-Net		0.7838	0.9823
75%	0.68	U-Net	✓	0.8054	0.9929
75%	0.68	Residual-UNet		0.8699	0.9882
75%	0.68	Residual-UNet	✓	0.8769	0.9889
75%	0.68	RAR-U-Net		0.9314	0.9939
75%	0.68	RAR-U-Net	✓	0.9380	0.9945
50%	0.77	U-Net		0.9202	0.9929
50%	0.77	U-Net	✓	0.9206	0.9930
50%	0.77	Residual-UNet		0.9012	0.9913
50%	0.77	Residual-UNet	✓	0.9327	0.9941
25%	0.85	U-Net		0.9268	0.9937
25%	0.85	U-Net	✓	0.9284	0.9938
25%	0.55	U-Net		0.8904	0.9901
25%	0.55	U-Net	✓	0.9073	0.9919
25%	0.55	Residual-UNet		0.9029	0.9915
25%	0.55	Residual-UNet	✓	0.9186	0.9929

that could create even the appearance of bias in the published work.

6. REFERENCES

- [1] O Ronneberger et al., “U-net: Convolutional networks for biomedical image segmentation,” in *Int Conf Med Im Comp & Comp-Assisted Intervention*. Springer, 2015, pp. 234–241.
- [2] M Kolařík et al, “Optimized high resolution 3d dense-u-net network for brain and spine segmentation,” *Applied Sciences*, vol. 9, no. 3, pp. 404, 2019.
- [3] K He et al, “Deep residual learning for image recognition,” in *Proc IEEE CVPR*, 2016, pp. 770–778.
- [4] Nabil Ibtehaz and M Sohel Rahman, “Multiresunet: Rethinking the u-net architecture for multimodal biomedical image segmentation,” *Neural Networks*, vol. 121, pp. 74–87, 2020.
- [5] O Oktay et al., “Attention u-net: Learning where to look for the pancreas,” *arXiv preprint arXiv:1804.03999*, 2018.
- [6] S Woo et al., “Cbam: Convolutional block attention module,” in *Proc ECCV*, 2018, pp. 3–19.
- [7] J Huang et al., “O2u-net: A simple noisy label detection approach for deep neural networks,” in *Proc IEEE ICCV*, 2019, pp. 3326–3334.
- [8] Pavel Yakubovskiy, “Segmentation models,” https://github.com/qubvel/segmentation_models, 2019.
- [9] V Yeghiazaryan et al., “Family of boundary overlap metrics for the evaluation of medical image segmentation,” *SPIE JMI*, vol. 5, no. 1, pp. 015006, 2018.
- [10] J Yao et al, “Detection of vertebral body fractures based on cortical shell unwrapping,” in *Int Conf Med Im Comp & Comp-Assisted Intervention*. Springer, 2012, pp. 509–516.